CrossMark

Hadron detection with a dual-readout fiber calorimeter

S. Lee [n], A. Cardini [c], M. Cascella [d], S. Choi [e], G. Ciapetti [h,i,1], R. Ferrari [f], S. Franchino [j],
M. Fraternali [f,g], G. Gaudio [f], S. Ha [e], J. Hauptman [k], H. Kim [n], A. Lanza [f], F. Li [k], M. Livan [f,g],
E. Meoni [l,m], J. Park [n], F. Scuri [b], A. Sill [a], R. Wigmans [a,*]

[a] Texas Tech University, Lubbock (TX), USA
[b] INFN Sezione di Pisa, Italy
[c] INFN Sezione di Cagliari, Monserrato (CA), Italy
[d] University College, London, UK
[e] Korea University, Seoul, Republic of Korea
[f] INFN Sezione di Pavia, Italy
[g] Dipartimento di Fisica, Università di Pavia, Italy
[h] Dipartimento di Fisica, Università di Roma "La Sapienza", Italy
[i] INFN Sezione di Roma, Italy
[j] Kirchhoff-Institut für Physik, Ruprecht-Karls-Universität Heidelberg, Germany
[k] Iowa State University, Ames (IA), USA
[l] Dipartimento di Fisica, Università della Calabria, Italy
[m] INFN Cosenza, Italy
[n] Kyungpook National University, Daegu, Republic of Korea

ARTICLE INFO

ABSTRACT

In this paper, we describe measurements of the response functions of a fiber-based dual-readout calorimeter for pions, protons and multiparticle "jets" with energies in the range from 20 to 180 GeV. The calorimeter uses lead as absorber material and has a total mass of 1350 kg. It is complemented by leakage counters made of scintillating plastic, with a total mass of 500 kg. The effects of these leakage counters on the calorimeter performance are studied as well. In a separate section, we investigate and compare different methods to measure the energy resolution of a calorimeter. Using only the signals provided by the calorimeter, we demonstrate that our dual-readout calorimeter, calibrated with electrons, is able to reconstruct the energy of proton and pion beam particles to within a few percent at all energies. The fractional widths of the signal distributions for these particles (σ/E) scale with the beam energy as $30\%/\sqrt{E}$, without any additional contributing terms.

© 2017 Elsevier B.V. All rights reserved.

1. Introduction

The performance of hadron calorimeters is typically strongly dominated, and negatively affected, by the effects of fluctuations in the electromagnetic (em) shower fraction, f_{em}. One approach to eliminate the effects of such fluctuations is to *measure* f_{em} for each event. It turns out that the Čerenkov mechanism provides unique opportunities in this respect. Calorimeters that use Čerenkov light as signal source are, for all practical purposes, only responding to the em fraction of hadronic showers [1]. By comparing the relative strengths of the signals representing the visible deposited energy and the Čerenkov light produced in the shower absorption process, the em shower fraction can

be determined and the total shower energy can be reconstructed using the known e/h value(s) of the calorimeter.[2] This is the essence of what has become known as *dual-readout* calorimetry. We are studying the properties of particle detectors of this type in the context of CERN's RD52 project [2].

In the dual-readout calorimeter discussed in this paper, signals are generated in scintillating fibers, which measure the deposited energy,

---

[2] The ratio e/h represents the ratio of the average calorimeter signals per unit deposited energy from the em and non-em components of hadron showers. A calorimeter with $e/h = 1$ is said to be *compensating*, but in practice almost all calorimeters have $e/h > 1$.

---

* Corresponding author. Fax: +1 806 742 1182.
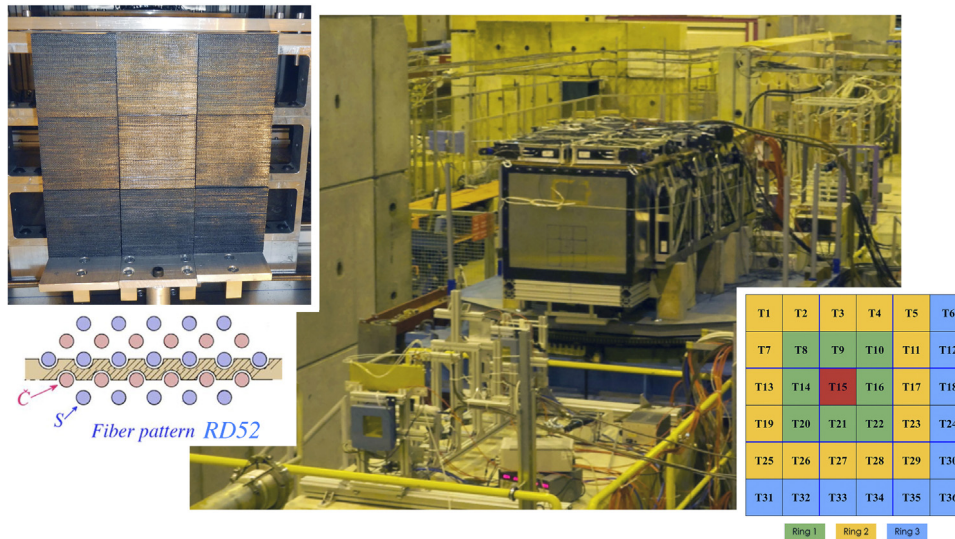 *E-mail address:* wigmans@ttu.edu (R. Wigmans).
[1] Deceased.

Fig. 1. Experimental setup in the H8 beam of the SPS at CERN. The calorimeter is installed inside a light tight box, surrounded on 4 sides by 20 modular leakage counters. The entire setup is installed on a movable table, which allows the impact point and the incident angle of the beam particles to be chosen as needed. The beam particles arrive through the vacuum pipe visible in the bottom left corner, and pass through several beam defining elements upstream of the calorimeter. The left inset shows a picture of the front face of the calorimeter, which consists of a 3×3 matrix of modules, and the arrangement of the scintillating and Čerenkov fibers in the lead absorber. The right inset shows the tower structure, one central tower surrounded by two complete rings and one incomplete one.
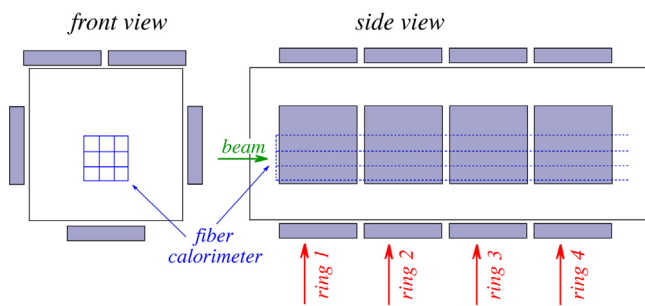

Fig. 2. Location of the leakage counters with respect to the fiber calorimeter. The front view shows that five counters form a "ring" around the calorimeter, the side view shows that there are four such "rings", located at different depths.

and in clear plastic fibers, which measure the relativistic shower particles, by means of the Čerenkov light generated by these. A large number of such fibers are embedded in a metal absorber structure. This detector is longitudinally unsegmented, the fibers are oriented in *approximately* the same direction as the particles to be detected. In previous papers, we have focused on the electromagnetic performance of such a detector [3,4] and on its capability to identify the particles developing showers in it [5].

In this paper, we describe experiments in which the hadronic performance of this calorimeter was measured. Hadron showers require a very large volume to fully develop. The 1350 kg fiducial volume of the calorimeter used for our purpose absorbed in practice, on average, only ∼90% of the shower, depending on the energy of the showering particle. Therefore, fluctuations in (side) leakage formed a dominating contribution to the energy resolution. In order to get a handle on this contribution, the calorimeter was surrounded by a (rather crude) system of leakage counters. In our measurements, we also tried to distinguish between showers initiated by pions and by protons, using the calorimeter information. Our experimental program concentrated on two issues:

(1) To what extent can the very crude system of leakage counters that we had installed around the calorimeter measure these event-to-event fluctuations and improve the measured energy resolution?

(2) Can we separate pions and protons in the CERN SPS H8 beam, and measure the dual-readout calorimeter performance separately for these particles?

We also studied the performance for multi-particle "jets", produced in high-multiplicity interactions by the beam hadrons in an upstream target. In modern particle physics experiments, the detection of jets is very important. The multiparticle events we used for our studies are, of course, not the same as the QCD jets that originate from a fragmenting quark or gluon. Yet, for the purpose of calorimetry they are very useful, since they represent a collection of particles that enter the calorimeter simultaneously. The composition of this collection is unknown, but the total energy is known. In the absence of a jet test beam, this is a reasonable alternative.

In Section 2, the instruments and the experimental setup in which the measurements were carried out are described, as well as the calibration and data analysis methods that were used. Experimental results are presented in Section 3. In Section 4, we investigate and compare different methods to measure the energy resolution of this calorimeter. Conclusions from these studies are presented in Section 5.

2. Equipment and measurements

2.1. Detectors and beam line

For these particular studies, which were carried out in October 2015, we used secondary or tertiary beams derived from the 400 GeV proton beam delivered by the CERN Super Proton Synchrotron. These particle beams were steered through the H8 line into the RD52 fiber calorimeter. Fig. 1 shows the experimental setup.

The fiber calorimeter used for the studies described in this paper is modular, and uses lead as the absorber material. Each of the nine modules is 2.5 m long (10 λ_{int}), has a cross section of 9.2×9.2 cm^2 and a fiducial mass of 150 kg. Each module consists of four towers ($4.6 \times 4.6 \times 250$ cm^3), and each tower contains 1024 plastic optical fibers (diameter 1.0 mm, equal numbers of scintillating and clear plastic fibers).[3] Each tower produces two signals, a scintillation signal and a

---

[3] The scintillating fibers are of the SCSF-78 type, produced by Kuraray, the Čerenkov light is generated in PMMA-based SK40 fibers, produced by Mitsubishi.

Čerenkov signal, which are detected by separate PMTs.[4] For this reason, this type of detector is also known as a DREAM (Dual-REAdout Method) calorimeter. The sampling fraction for minimum ionizing particles in this calorimeter, both for the scintillation and for the Čerenkov sampling structure, is 5.3%.

Measurements of the radial shower profile showed that the showers initiated by 60 GeV π^- were, on average, contained at the level of ∼93% in this structure. Electromagnetic showers are contained to better than 99% and shower leakage was thus not an issue for electrons and photons. In order to detect the hadronic shower leakage, the calorimeter was surrounded by large slabs of plastic scintillator ($50 \times 50 \times 10$ cm^3, mass 25 kg). Twenty such counters were used in these tests. They can be seen in Fig. 1 on the top, the bottom and the right hand side of the box containing the calorimeter. The location of the leakage counters with respect to the fiber calorimeter is shown in Fig. 2.

The experimental setup also contained a number of auxiliary detectors, which were intended to limit and define the effective size of the beam spot, to determine the identity of individual beam particles, and to measure their trajectory. Fig. 3 shows a schematic overview of the beam line, in which the positions of these auxiliary counters are indicated (not to scale):

- A set of three small scintillation counters provided the signals that were used to trigger the data acquisition system. These trigger counters were 2.5 mm thick, the area of overlap between the first two (T_1, T_2) was 4×4 cm^2. Downstream from these counters, a third scintillation counter (T_H) was installed. The latter had a hole with a radius of 10 mm in it. A (anti-)coincidence between the logic signals from these counters provided the trigger ($T_1 \cdot T_2 \cdot \overline{T_H}$).
- The trajectories of individual beam particles could be reconstructed with the information provided by two small delay wire chambers (DC1, DC2). This system made it possible to determine the location of the impact point of 80 GeV beam particles at the calorimeter surface with a precision of about 1 mm.
- About 80 cm upstream of the calorimeter, a preshower detector (PSD) provided signals that could be used to remove electrons contaminating the hadron beams. This PSD consisted of a 5 mm thick lead plate, followed by a 5 mm thick plastic scintillator. Electrons started developing showers in this device, while muons and hadrons typically produced a signal characteristic of a minimum ionizing particle (mip) in the scintillator plate.
- For certain energies, an interaction target (IT), consisting of 10 cm of plastic, followed by a 5 mm thick plastic scintillator, was installed behind the PSD. This detector was used to create and select interactions in the plastic in which a significant number of secondaries were produced. The signal in the scintillator provided a means to select events with a certain (minimum) multiplicity.
- Downstream of the calorimeter, a Tail Catcher (TC) could also serve to help identify pions and muons. This Tail Catcher consisted of a simple 20×20 cm^2 scintillation counter. Electrons were fully absorbed in the calorimeter and thus did not create a signal in this detector, while muons produced a mip signal in it. Larger signals were typically caused by late showering hadrons.
- Further downstream of the calorimeter, behind an additional $8\lambda_{\text{int}}$ worth of absorber, a 50×50 cm^2 scintillation counter (μ) served to identify muons that contaminated the particle beam.
- About 50 m upstream of the calorimeter, two Threshold Čerenkov counters ($\check{C}_{1,2}$) provided signals that made it possible to identify the type of beam particle. These counters were filled with CO_2 gas at a pressure that was chosen depending on the beam energy. These counters were in practice used to separate pions from protons.

The calorimeter was mounted on a table that could be displaced both horizontally and vertically, and also rotated around the vertical axis. This allowed us to choose both the impact point and the angle of incidence of the beam particles.

2.2. Data acquisition

In order to minimize delays in the DAQ system, short, fast cables were used to transport the signals from the trigger counters to the counting room. All other signals were transported through standard RG-58 cables with (for timing purposes) appropriate lengths.

In the counting room, signals from the Threshold Čerenkov counters, PSD, Interaction Target, Tail Catcher and muon counter were fed into charge ADCs. The signals from the wire chambers were fed into TDCs. The data acquisition system used VME electronics. Two VME crates hosted all the needed readout and control boards. The signals from the 72 calorimeter channels, the 20 leakage counters and the auxiliary detectors (Threshold Čerenkov counters, PSD, Interaction Target, Tail Catcher, and Muon counter) were integrated and digitized with a sensitivity of 100 fC/count and a 12-bit dynamic range on four 32-channel CAEN QDC modules (V862AC, V792AC). The timing information of the tracking chambers was recorded with 1 ns resolution in a 16-channel CAEN V775N TDC, and was converted into (x, y) coordinates of the point where the beam particle traversed the chamber. All information was collected using a gate width of 100 ns, and read out event-by-event through the V2718 CAEN optical link bridge with a dead time of ∼300 μs. The event rates were such that pileup effects were negligible.

Our readout scheme optimized the CPU utilization and the data taking efficiency using the bunch structure of the SPS accelerator cycle (which lasted between 36 and 54 s, depending on the various tasks of the accelerator complex), during which period beam particles were provided to our experiment by means of two extractions with a duration of 4.8 s each.

2.3. Experimental data, calibration and analysis methods

The measurements described in this paper were performed in the H8 beam line of the Super Proton Synchrotron at CERN. We used either secondary beams directly produced by the 400 GeV protons from the accelerator on a target shared by several beam lines, or tertiary beams derived from these secondary ones. For the experiments described in this paper, a secondary beam of 20 GeV positive particles was used to calibrate all calorimeter towers. This beam consisted almost exclusively of positrons. Secondary beams of 60 and 180 GeV were used to measure the hadronic response functions at a variety of energies. Low energy beams were derived as tertiaries from the 60 GeV secondary beam, and beams with energies above 60 GeV were derived from the 180 GeV secondary beam. The latter was also used to provide 180 GeV μ^+ particles (obtained by blocking all other particles with upstream absorbers), which were used to calibrate the leakage counters. The tertiary beams had a mixed composition (see Table 1) and, as described below, dedicated efforts were made to extract non-biased hadron event samples from the collected data.

For the calibration runs, the 20 GeV positron beam was steered into the center of each of the 36 individual calorimeter towers (see inset Fig. 1), or through the central plane of the leakage counters. For each run, 10 000 events were collected, while 10% randomly triggered events provided pedestal information. The information from the wire chambers was used to select events in which the particles hit the calorimeter within a beam spot with a diameter of 10 mm. The high voltage settings were chosen such that the average calorimeter signal corresponded to several hundred ADC counts. The calibration runs were used to determine the energy equivalent of one ADC count for all individual signals, *i.e.,* the 36 scintillation signals, the 36 Čerenkov signals and the 20 signals from the leakage counters. These calibration constants formed the basis for the energy determination of the hadronic events. The 72
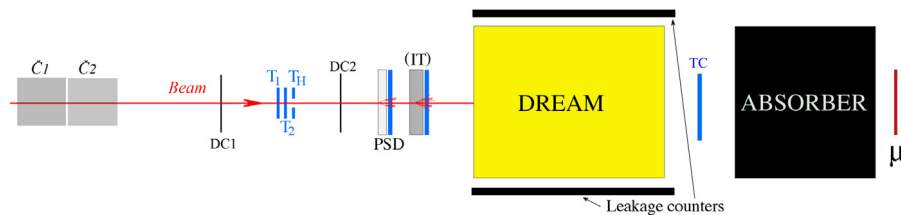

Fig. 3. Schematic layout of the experimental setup (not to scale). Shown are the Threshold Čerenkov counters (Č1, Č2), the delay wire chambers (DC1, DC2), the trigger counters (T₁, T₂, T_H), the preshower detector (PSD), the Interaction Target (IT), the calorimeter surrounded by leakage counters, the Tail Catcher (TC) and the Muon counter (μ). See text for more details.

Table 1
Percentage of events that qualified as electrons, muons, pions and protons. The proton percentage is a maximum. It contains a possible contamination (misidentified pions) that is listed as well. See text for more details.

Beam energy (GeV)	Electrons	Muons	Pions	Protons	Possible contamination of p
+10	62%	–	38%	–	–
+20	31%	0.9%	58%	10%	–
+40	41%	1.9%	41%	16%	3%
+60	30%	1.8%	44%	24%	3%
−60	23%	0.9%	76%	–	–
+80	20%	2.7%	36%	41%	4%
+100	14%	4%	20%	62%	–
+125	5%	40%	10%	45%	–
+180	–	1%	2%	97%	–

calibration constants of the calorimeter towers were determined with 20 GeV positrons, which deposited 93% of their energy in one individual tower. The calibration constants of the leakage counters were equalized using 180 GeV muons which traversed the 50 cm long central plane of each counter. The overall scale of the leakage signals was set with 60 GeV pions sent into the center of the calorimeter. The total signal from all leakage counters combined was set to 3.84 GeV, representing 6.4% of the particle energy.[5] In the analysis of the hadronic calorimeter performance described in the following sections, the scintillation signal is the sum of the signals measured in the scintillating fibers embedded in the calorimeter and the signals from the leakage counters, both expressed in GeV, using the scale derived from the electron calibration. This scale was also used for the hadron signals from the Čerenkov fibers. The electron calibration thus formed the basis for the conversion of *all* signals produced by this calorimeter into deposited energy.

Dedicated hadron runs were carried out for the following energies and polarities: +20, +40, ±60, +80, +100, and +125 GeV. Dedicated multiparticle ("jet") runs were performed at +40, +60, +100 and +125 GeV. In all cases, the particle beam was steered into the center of T15 (see Fig. 1). For each event selected by the trigger counters, the ADC data from the auxiliary detectors and the wire chamber information were recorded. Off-line, this beam chamber information was used to select events within a small beam spot (typically with a radius < 5 mm). The information provided by the auxiliary detectors was used to identify and select the desired particles.

In order to select hadron event samples, the electrons and muons had to be removed from the collected events. This had to be done in a way that would not bias the resulting hadron event samples, and therefore had to be based entirely on the auxiliary detectors. Electrons (or positrons) were identified as particles that produced a signal in the PSD that was larger than ∼200 ADC counts above pedestal, which corresponds to the combined signals produced by two minimum ionizing particles (mips) traversing this detector. Additional requirements were that no signals incompatible with electronic noise were produced in the muon counter. Muons were identified as particles that produced a signal incompatible with electronic noise in the muon counter. At low energies,

a significant fraction of the muons did not traverse that counter because of multiple scattering (or absorption) in the upstream material. In that case, particles were also identified as muons if they produced signals in the PSD or IT, as well as in the Tail Catcher, that were compatible with a mip, and no signal incompatible with the pedestal in the sum of all leakage counters.

Protons were defined as particles that produced a signal compatible with the pedestal in both upstream Threshold Čerenkov counters. Pions were required to produce a signal in at least one of these counters that was significantly (at least 3σ) above pedestal. Table 1 lists the percentages of protons and pions in the hadron event samples determined on the basis of this criterion, as well as the percentage of contaminating electrons and muons.

The counters were not fully efficient, and therefore the resulting proton/pion separation was not perfect, especially at the highest energies. Fig. 4 shows the signal distributions measured for beams of +40 and +100 GeV.

In order to determine the inefficiency of the Threshold Čerenkov counters, we compared the signal distributions measured for beams with negative and positive polarity at the same energy. This comparison assumes that the production of antiprotons on the production target is negligible. Table 2 shows the fraction of hadrons (*i.e.,* after electrons and muons have been removed from the event samples) that produced signals compatible with the pedestal in *both* Threshold Čerenkov counters, for beams of 40, 60 and 80 GeV.

Based on these considerations, we estimated the purity of the proton sample. The possible contamination of the proton sample by misidentified pions is listed in the last column of Table 1, as a percentage of the total number of events. The negative polarity hadrons were all considered pions. No attempts were made to measure the contribution of kaons to the various event samples. Such contributions are estimated (from beam simulations) to be at the few percent level. Since kaons would also generate pedestal events in the Threshold Čerenkov counters, the percentage of protons listed in Table 1 is a maximum.

No distinction was made between protons and pions for the measurements with the Interaction Target. Interacting hadrons were selected by means of a cut in the signal from the scintillation plate connected to the downstream end of this plastic target. An interacting hadron was defined as an event in which a signal compatible with a mip was produced in the PSD, combined with a signal larger than a certain minimum value (equivalent to 6 mips) in the IT.

Table 2
Percentage of hadronic events with pedestal signals in *both* Threshold Čerenkov counters.

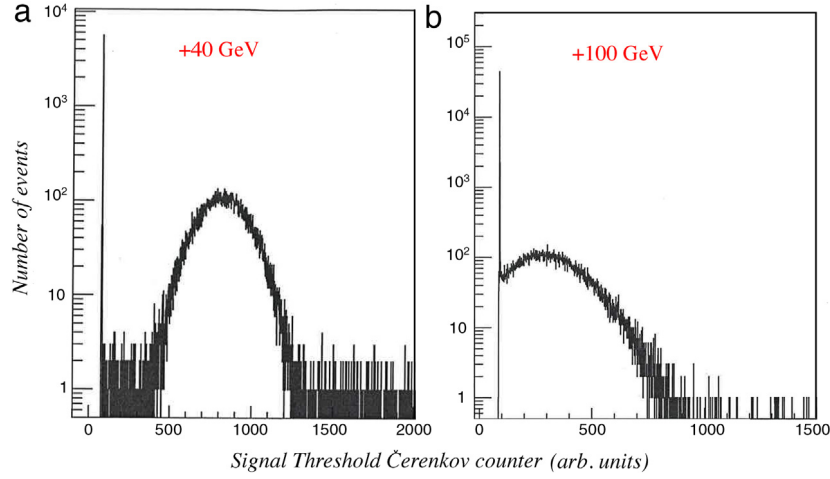| Beam energy (GeV)	Pedestals in $\check{C}_1, \check{C}_2$	Beam energy (GeV)	Pedestals in $\check{C}_1, \check{C}_2$
+40	27.3%	−40	5.1%
+60	35.0%	−60	3.6%
+80	53.5%	−80	4.6%

Fig. 4. Signal distributions in one of the Threshold Čerenkov counters for positive particles of 40 GeV (a) and 100 GeV (b). The gas pressure was such that protons would *not* produce a signal, but pions would.

3. Experimental results

3.1. The dual readout method

The Dual-Readout approach for measuring hadron showers exploits the fact that the energy carried by the non-em shower component of hadron showers is mostly deposited by non-relativistic shower particles (protons), and therefore does not contribute to the signals of a Čerenkov calorimeter. By measuring simultaneously the visible deposited energy (dE/dx) and the Čerenkov light generated in the shower absorption process, one can determine $f_{\rm em}$ *event by event* and thus eliminate (the effects of) its fluctuations. The correct hadron energy can be determined from a combination of both signals.

This principle was first experimentally demonstrated by the DREAM Collaboration [6], with a Cu/fiber calorimeter. Scintillating fibers measured dE/dx, and quartz fibers measured the Čerenkov light. The response ratio of these two signals was related to $f_{\rm em}$ as

$$\frac{C}{S} = \frac{f_{\rm em} + 0.21\,(1 - f_{\rm em})}{f_{\rm em} + 0.77\,(1 - f_{\rm em})} \tag{1}$$

where 0.21 and 0.77 represent the h/e ratios of the Čerenkov and scintillator calorimeter structures, respectively. The hadron energy could be derived directly from the two signals [7]:

$$E = \frac{S - \chi C}{1 - \chi}, \quad \text{with} \quad \chi = \frac{\left[1 - (h/e)_S\right]}{\left[1 - (h/e)_C\right]} \approx 0.3. \tag{2}$$

The e/h values, and thus the value of the parameter χ are a bit different when lead absorber is used.

3.2. Impact of the leakage counters

In order to study the effectiveness of the described leakage counters, we first studied the correlation between the signals from these counters and the scintillation signals from the fiber calorimeter. The result, shown in Fig. 5 for 60 GeV π^-, indicates that there is indeed a good anti-correlation between the *average* signals. However, the resolution improvement depends of course on the *event-by-event anti-correlation*. The counters turned out to be indeed somewhat effective in that respect.
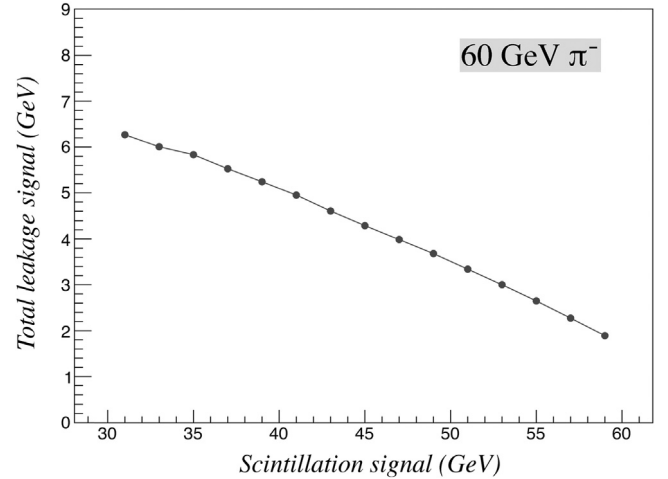

Fig. 5. Relationship between the average signals from 60 GeV π^- showers measured in the scintillation channels of the calorimeter and in the array of leakage counters.

An extreme example of this effectiveness is shown in Fig. 6, in which the signal distribution for all events (Figs. 6a) is compared with the signal distribution for the events in which *no* shower leakage was observed, *i.e.*, the (small fraction of the) events that were entirely contained in the fiber calorimeter. The latter distribution exhibits an energy resolution that is almost a factor of two better, and is in addition well described by a Gaussian function. These signal distributions were obtained with the standard dual-readout procedure (Section 3.1).

The signal distribution for all 60 GeV π^- events shows deviations from a Gaussian shape. The type of deviations indicates that effects of light attenuation in the (scintillating) fibers are responsible for this [8]. The response of the fibers is not uniform in depth. Because of light attenuation, the response gradually increases as the light is produced closer to the PMTs, *i.e.*, deeper inside the calorimeter. The convolution of the attenuation curve with the longitudinal light production profile in hadron showers leads to a response function with
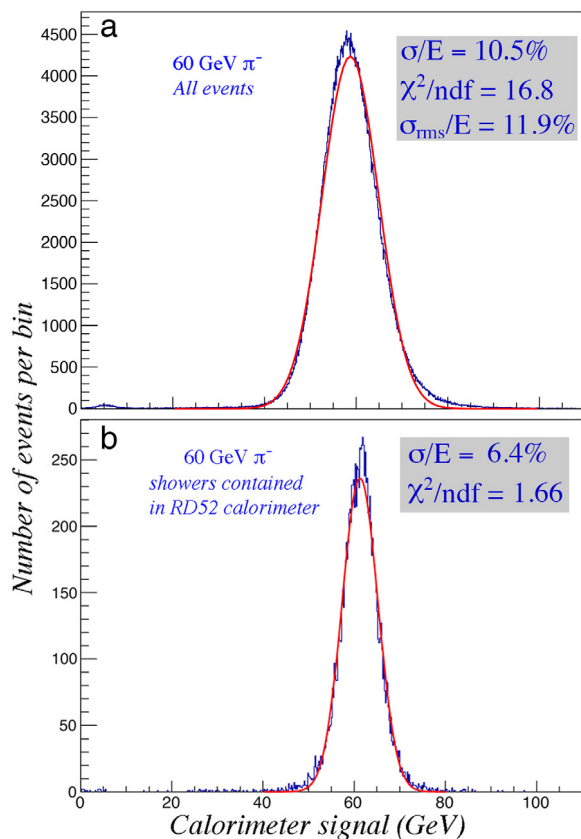
Fig. 6. Total signal distributions for 60 GeV π^-, measured with the dual-readout method. Shown are the distributions for all events (a) and for events that were fully contained inside the calorimeter, *i.e.,* for which no energy leakage was measured in the leakage counters (b).

the measured characteristics. The steeper the light attenuation curve, the more pronounced these effects become. It has been demonstrated that the effective light attenuation length increases with the distance to the light detector [9]. An important feature responsible for this is the "cladding light", which is much stronger attenuated than light trapped inside the fiber core. Therefore, this cladding light contributes predominantly to the signals from energy deposited close to the light detector. By making the upstream end of the fibers reflective, the attenuation curve becomes flatter, increasingly so as the distance to the light detector increases. In this way, effective attenuation lengths in excess of 8 m were obtained for the fibers in the SPACAL calorimeter [8]. However, in our calorimeter, the open end of the fibers was not made reflective, and the attenuation length is therefore shorter. The effect of this is an additional contribution to the hadronic energy resolution which, in first approximation, is energy independent. This contribution, as well as the asymmetry of the response function, increases as the light is produced closer to the PMTs, *i.e.,* deeper inside the calorimeter.

To investigate these phenomena, we separated the events into sub-samples, based on the fraction of the total leakage signal that was measured in ring 1 of the leakage counters (see Fig. 2). Fig. 7a shows the distribution of that fraction. In general, we may assume that a small fraction indicates that the scintillation light is, on average, produced deep inside the calorimeter, *i.e.,* in the region where the light attenuation curve is steeper than for light produced close to the calorimeter's front face [9].

Fig. 7b shows that the asymmetry is indeed predominantly observed for events in which that fraction is small (<0.2), *i.e.,* events in which most of the energy was deposited deep inside the calorimeter, where the effects of light attenuation are largest. The signal distributions for the other events are much more Gaussian (Fig. 7c). The average calorimeter

signal is also somewhat smaller for these events, which is consistent with larger attenuation losses due to the longer path length of the light on its way to the PMT. These results indicate that light attenuation in the scintillating fibers was indeed a significant factor contributing to the hadronic energy resolution of this calorimeter. By comparing Figs. 6a and 6b, one may conclude that leakage fluctuations contributed the rest.

In order to investigate how effective the signals from the leakage counters were in reducing the effects of side leakage on the energy resolution, we compared the signal distributions for the 60 GeV pions in which the leakage signals were added event by event to those from the scintillating fibers (Fig. 8a) with the signal distributions in which the fiber scintillation signals were all multiplied by a constant factor, representing the average leakage fraction (Fig. 8b). The leakage counters did indeed improve the hadronic energy resolution significantly, albeit not as much as one might expect from a sufficiently enlarged fiber calorimeter. If we take the energy resolution of 6.4% (Fig. 6b) as the value for fully contained showers,[6] then the contribution of leakage fluctuations to the resolution shown in Fig. 8 was reduced from 11.1% in the absence of any leakage detection (Fig. 8b) to 7.8% for the imperfect leakage detector used in these studies (Fig. 8a).

We have shown in the past that the light attenuation effects can be eliminated event by event through the time structure of the signals [5], or by placing the calorimeter at a small (~1°) angle with the beam line [6]. That information was not available during these tests. Instead, we have chosen to limit the analyses to event samples in which more than 20% of the leakage signal was recorded in the first ring of the leakage counters. A comparison of Figs. 7b and 7c shows that this cut selects about 30% of the events. This percentage is about the same for pions of other energies. For protons, the percentage is typically somewhat larger, which probably reflects the smaller interaction length. In the case of multiparticle events, the effective depth of the shower energy deposition is located much more upstream, and therefore the fraction of the events that are selected by this cut is larger than for single hadrons (~60%). A comparison of Figs. 7b and 7c also shows that this cut has indeed the effects of selecting a sample of events that start in the upstream section of the calorimeter. The scintillation signals from these events are, on average, 3.8% smaller than those from the discarded event sample because of the increased light attenuation. They also suffer considerably less from the effects of light attenuation fluctuations in the scintillating fibers, as evidenced by the χ^2 values of the Gaussian fit. Since one of our main goals was the study of the effects of shower leakage, we made this cut to eliminate the effects of light attenuation on the energy resolution as much as possible.

3.3. Proton/pion differences

A second issue we wanted to investigate with the data taken during the 2015 test beam period concerned the separation of pions and protons using *only* calorimeter information. To that end, we used the two threshold Čerenkov counters that were installed about 50 m upstream of the calorimeter setup. These counters were filled with CO_2 gas at a pressure that was chosen depending on the beam energy. Protons were defined as particles that produced a signal compatible with the pedestal in both Čerenkov counters. Pions were required to produce a signal significantly (at least 3σ) above pedestal in at least one of these counters (see Fig. 4).

In 1998, Akchurin and coworkers showed that there are significant differences between the shower development of high-energy protons and pions, which have measurable consequences for the signals from non-compensating calorimeters [11]. In prototype studies of the Forward Calorimeter for CMS, which is based on the detection of Čerenkov light, they found that the signals from pions were typically ~10% larger than those from protons of the same energy. On the other hand, event-to-event fluctuations in these signals were ~10% smaller for protons, and

---

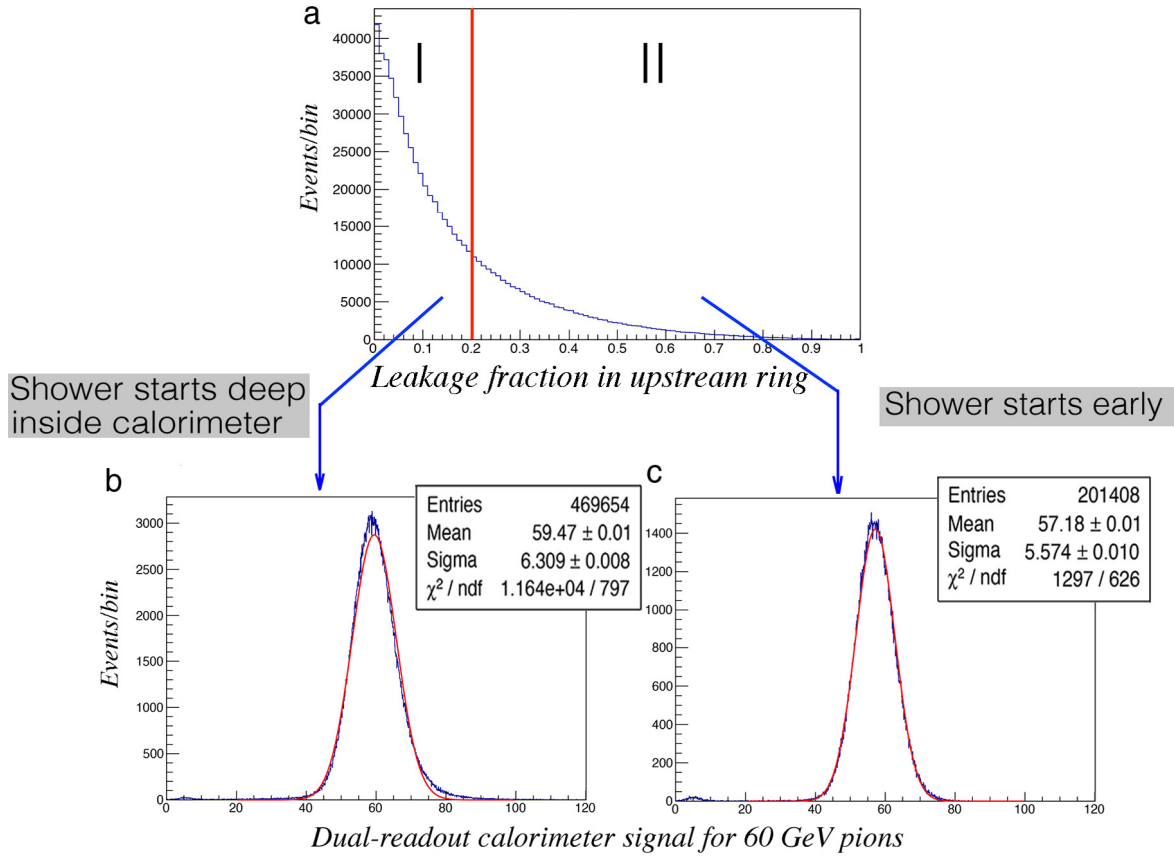[6] GEANT4 based Monte Carlo simulations gave similar resolution values [10].

Fig. 7. Signal distributions for 60 GeV π^- measured with the dual-readout method (b, c), for different cuts on the fraction of the total leakage signal that was recorded in the first ring of the leakage counter array (a). The energy scale is expressed in units of GeV, as established in the calibration with electrons. See text for more details.
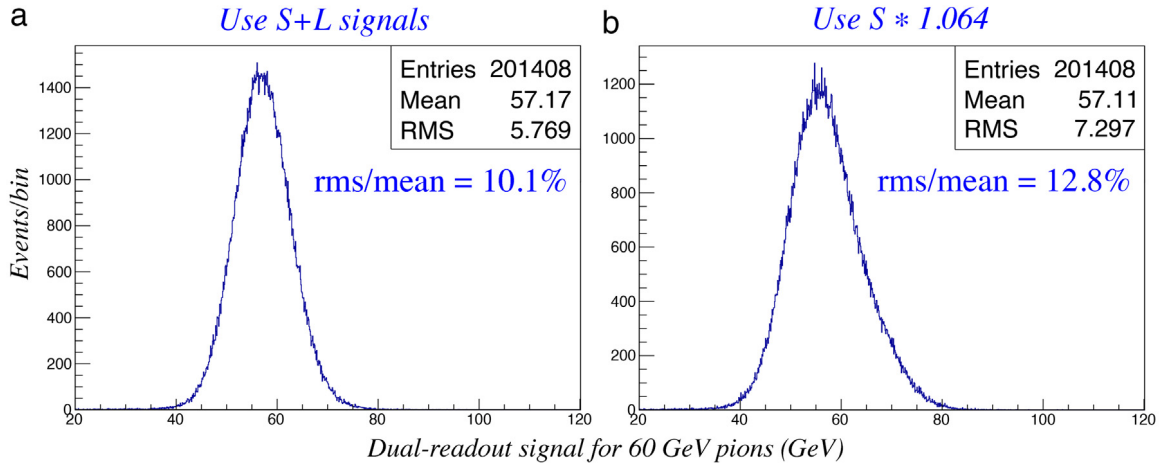

Fig. 8. Signal distributions for 60 GeV π^-, measured with the dual-readout method. The scintillation signal from the fibers was increased with the total signal measured in the leakage counters (a), or simply multiplied by a factor of 1.064 for all events (b).

the signal distributions were also more symmetric for protons. These differences are a consequence of the requirement of baryon number conservation, which prohibits a π^0 from being the leading particle in proton induced showers.

Our data are in agreement with these findings. Fig. 9 shows signal distributions for the Čerenkov signals from 80 GeV pions (9a) and 80 GeV protons (9b), respectively. Indeed, the proton signals are, on average, ~10% smaller than the pion ones. On the other hand, the signal distribution for the protons is more symmetric and also somewhat narrower than the pion one. Interestingly, a comparison between Figs. 9c and 9d shows that application of the dual-readout method (Eqs. (1)

and (2)) largely eliminated the differences between these two types of showers.

3.4. The calorimeter performance for single hadrons

In this section, we present results on the energy resolution measured for single hadrons of different energies. For the positive polarity, separate samples of protons and pions were used. No attempts were made to isolate the kaons, whose showers should also be different from pion ones in terms of the em shower component. Strangeness conservation prevents the production of leading π^0s in kaon induced
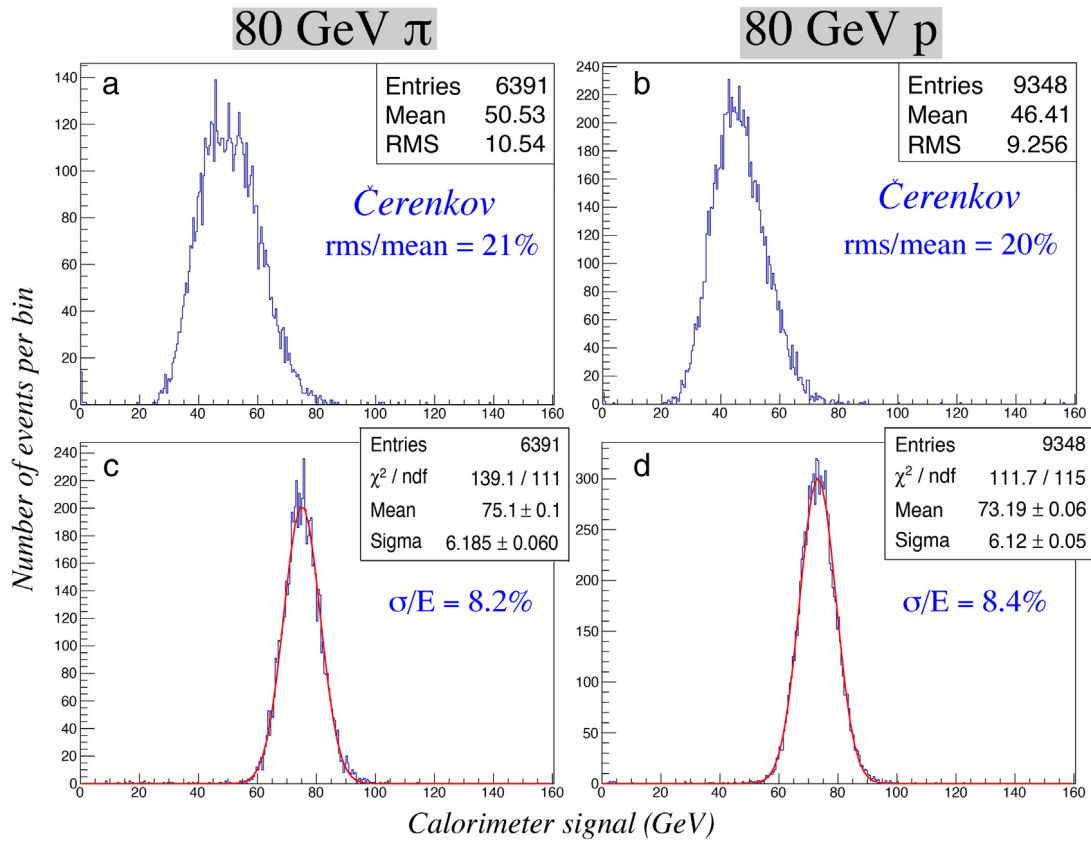
Fig. 9. Signal distributions for 80 GeV pions and protons measured with the 9-module lead-based fiber calorimeter. Shown are the distributions for the Čerenkov signals from 80 GeV π^+ (a) and protons (b), as well as the dual-readout total signals for 80 GeV π^+ (c) and protons (d).
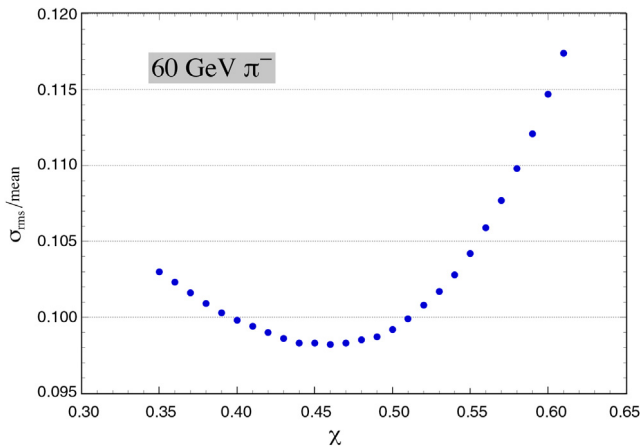

Fig. 10. The energy resolution ($\sigma_{rms}/mean$) obtained with the dual-readout method, as a function of the value of the parameter χ in Eq. (2), for 60 GeV π^-.

showers, and therefore the characteristics of the em shower component (average value, event-to-event fluctuations in f_{em}) are probably similar to those in proton induced showers.

For every event, two signals were available, a Čerenkov signal and a scintillation signal. The particle energy was found by combining these signals as in Eq. (2), using a parameter value $\chi = 0.45$. Both the reconstructed energy and the quality of the Gaussian fit are sensitive to the value of this parameter, and the chosen value represents the result of an optimization procedure in which χ was varied in small steps (Fig. 10).

The optimal value is somewhat larger than for the copper-based DREAM calorimeter, as a result of differences between the e/h values for

lead and copper, both for the scintillation and the Čerenkov sampling structure [12]. We have used a value $\chi = 0.45$ for our lead-based calorimeter throughout this analysis. The procedures to obtain signal distributions for pions and protons were identical over the entire energy range studied here.

As an example, Fig. 11 shows the distributions for the two individual signals, as well as the distribution of the dual-readout signals, combined according to Eq. (2), for 20 GeV pions. These distributions illustrate the benefits of the dual-readout method. Whereas the C and S distributions are rather wide and asymmetric, the dual-readout signal distribution is well described by a Gaussian fit.

The results of this study are summarized in Figs. 12 and 13. Fig. 12 shows the average signal per unit deposited energy (*i.e.*, the calorimeter response) as a function of energy, for pions with energies ranging from 20 to 125 GeV. Results are given separately for the Čerenkov signals and for the dual-readout signals. Whereas the Čerenkov response increased by more than 50% over this energy range, the dual-readout response was constant to within a few percent, except for the lowest energy. The results for protons were essentially the same.

The hadronic energy resolution is shown as a function of energy in Fig. 13. The energy scale is proportional to $-E^{-1/2}$, which means that the data points should be located on a straight line through the bottom right corner of this plot if the resolution is only determined by fluctuations that are governed by Poisson statistics. Any deviation from such a line means that non-stochastic effects play a significant role. The experimental data show that the energy resolution for pions is well described by *stochastic fluctuations alone* when the dual-readout signals are considered.[7] On the other hand, the energy resolution measured on the basis of the Čerenkov signals exhibits substantial deviations from

---

[7] Our Monte Carlo simulations have shown that this energy resolution is dominated by fluctuations in lateral shower leakage [10].
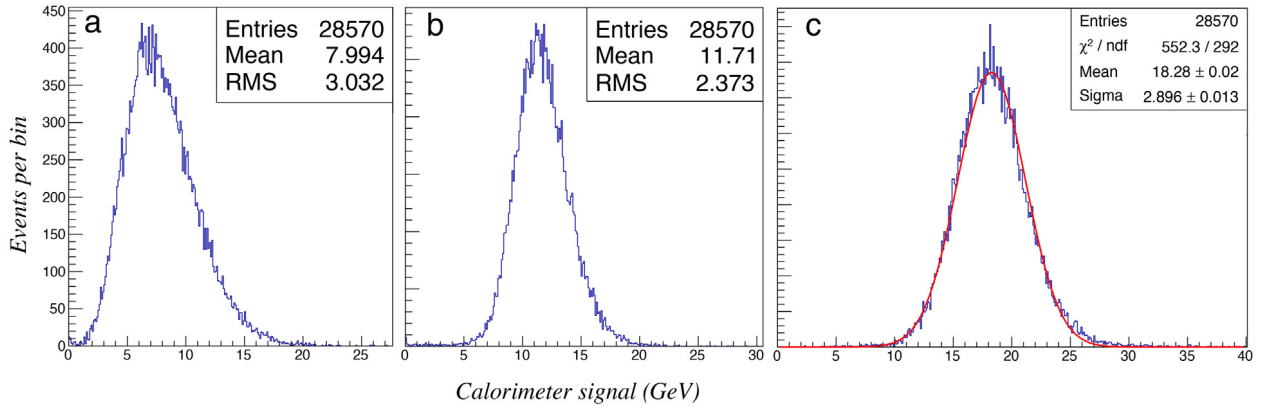
Fig. 11. Signal distributions for 20 GeV π^- particles. Shown are the measured Čerenkov (a) and scintillation (b) signal distributions as well as the signal distribution obtained by combining the two signals according to Eq. (2), using $\chi = 0.45$ (c).
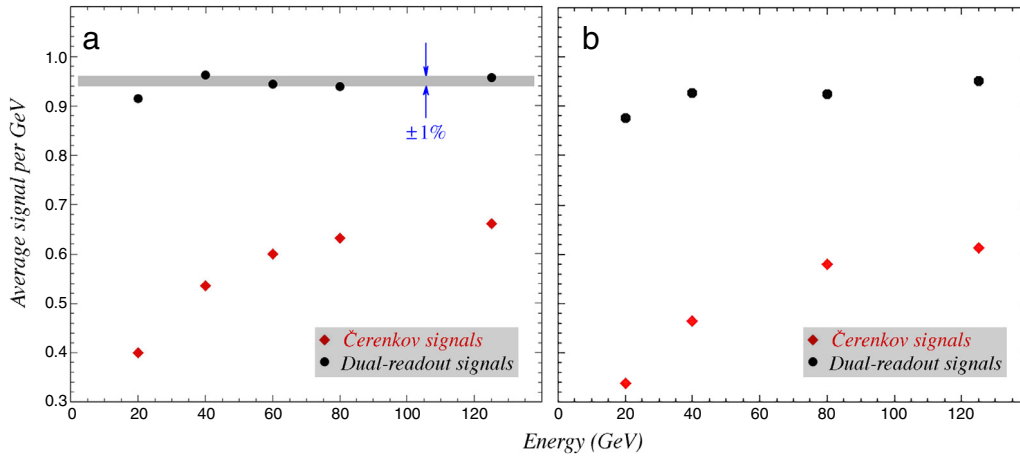

Fig. 12. The hadronic response of the RD52 lead–fiber dual-readout calorimeter, for single pions (a) and protons (b). Shown are the average Čerenkov signal and the dual-readout signal (Eq. (2)) per unit deposited energy, as a function of the energy.
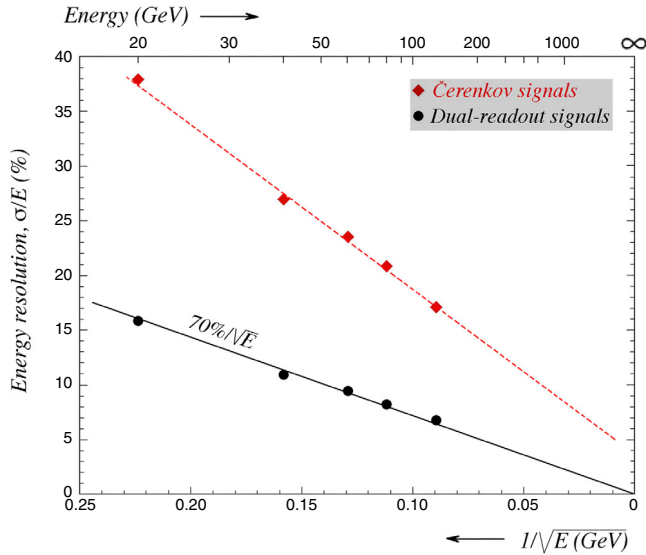

Fig. 13. The hadronic energy resolution of the RD52 lead–fiber dual-readout calorimeter, for single pions. Shown are the results for the Čerenkov signals alone, and for the dual-readout signals, obtained with Eq. (2).

$E^{-1/2}$ scaling. The straight line fit through the experimental data points suggests a 5% resolution at infinite energy. This is a consequence of the

fact that the event-to-event fluctuations in the em shower fraction (f_{em}) are not stochastic.

The statistical errors on the results presented in Figs. 12 and 13 are smaller than the size of the data points in these figures. Sources of systematic errors include

- The value of the dual-readout parameter χ (Eq. (2)). We have varied the value of this parameter between 0.4 and 0.5 (see Fig. 10), and found that the energy resolutions changed only by 1%–2%. On the other hand, the reconstructed energy varied by 4%–5% over this parameter range. The effect is larger since the reconstructed energy continuously increases with the value of χ, while the energy resolution reaches a minimum value in the chosen parameter range.
- The effects of light attenuation. Hadronic showers deposit their energy deeper inside the calorimeter than the electrons that were used to calibrate the signals. Because of light attenuation in the fibers, the signals increase when the light is produced closer to the PMTs, i.e., deeper inside the calorimeter. This is illustrated in Fig. 7. Because we selected event samples in which more than 20% of the total leakage signal was produced in the first ring of leakage counters, the effects of light attenuation were limited, in two ways. First, the event-to-event fluctuations in light attenuation were reduced, thus minimizing the effect on the energy resolution and the shape of the response function. Second, the difference between the hadronic and electronic energy scales was minimized. Based on the light attenuation characteristics of the fibers, we estimated this difference to be about 2%.

- The calibration of the leakage counter signals. This calibration was based on a measurement of the lateral shower profile for 60 GeV pions, which revealed that on average 6.4% of the shower energy leaked out sideways [13], and this result was used to set the energy scale for the signals from the leakage counters. In doing so, it was implicitly assumed that the Čerenkov light produced in the shower development was entirely contained in the fiber calorimeter. However, since there is no way in which we could possibly separate the signals from the leakage counters into scintillation and Čerenkov components, there is no good alternative. In any case, the main effect of this systematic effect would be a change in the optimal χ value, the consequences of which are discussed above.

4. The energy resolution of a calorimeter and how to determine it

4.1. Introduction

In this section, we look in detail at the meaning of the term *energy resolution* and discuss and compare various ways in which it is determined in practice. Strictly speaking, the energy resolution of a calorimeter describes the precision with which the energy of an unknown object that is absorbed in it can be determined. In practice, this important characteristic is usually measured with a beam of mono-energetic particles produced by an accelerator. This beam is sent into the detector. The (relative) energy resolution is deemed to be represented by the (fractional) width of the distribution of the signals produced by the calorimeter in response to these particles. Two important caveats should be mentioned in this context:

(1) Since all particles typically enter the calorimeter in the same small area defined by the beam spot, the results are strictly speaking only valid for this particular part of the calorimeter. If the average signal varies with the impact point of the particles, which is often the case, then the real energy resolution is underestimated in this procedure.

(2) The width of the signal distribution measured in this way is only indicative for the energy resolution if the average calorimeter signal indeed represents the correct energy of the beam particles. This condition may not be met, for example, when the calorimeter is intrinsically non-linear and has been calibrated at a different energy than that of the beam particles. It is also not met when the average signals are different for different types of particles with the same energy (*e.g.,* π, K, p) and the beam composition is unknown.

However, even when we assume that these caveats do not play a role for the calorimeter in question, one should realize that the procedure chosen to determine the energy resolution relies on the signal distribution from an ensemble of particles with the same energy. This is a crucial aspect of methods that attempt to improve the energy resolution by techniques known as *offline compensation*, or *Particle Flow Analysis*, where the width of a signal distribution is reduced with an iterative procedure, in which calibration constants of the various calorimeter sections that contribute to the signals are varied until an optimal result is obtained.

The procedure used to determine the energy resolution of the RD52 calorimeters, as described in the previous section, does *not* rely on the availability of an ensemble of events created by particles of the same energy. The particle energy is determined with a simple formula (2), which combines the values of two signals. The energy resolution is measured by comparing that calculated energy with the true energy of the particle that created the event. The availability of an ensemble of mono-energetic particles is not essential in this case.

However, if measuring the energy resolution is considered equivalent to measuring the width of the signal distribution for an ensemble

of mono-energetic beam particles, then the dual-readout method also offers an alternative approach, described below. This approach leads to resolutions that are considerably better than the ones mentioned in the previous section.

4.2. The rotation method for single hadrons

Fig. 14a shows a scatter plot of the Čerenkov signals *vs.* the scintillation signals measured with this detector for 60 GeV pions. The signals from the leakage counters were added to those from the scintillating fibers, using the fact that the measured shower profile indicated that the side leakage at this energy was, on average, 6.4%. The energy scale for both the Čerenkov and the scintillation signals is given in units of GeV, derived from the calibration of these signals with electron showers.

This scatter plot shows the data points located on a locus, clustered around a line that intersects the $C/S = 1$ line at the beam energy of 60 GeV. This is of course to be expected. In first approximation, the Čerenkov fibers only produced signals generated by the electromagnetic components of the hadron showers, predominantly π^0s. The larger the em shower fraction, the larger the C/S signal ratio. Events in which (almost) the entire hadronic energy was deposited in the form of em shower components thus produced signals that were very similar to those from 60 GeV electrons and are, therefore, represented by data points located near (60,60) in this scatter plot. The fact that the data points cluster around a straight line in this plot is in agreement with Groom's assessment of the fundamental aspects of dual-readout calorimetry [14].

We can now rotate the scatter plot over the angle θ around this intersection point:

$$\begin{pmatrix} S' \\ C' \end{pmatrix} = \begin{pmatrix} \cos\theta & -\sin\theta \\ \sin\theta & \cos\theta \end{pmatrix} \begin{pmatrix} S \\ C \end{pmatrix} \tag{3}$$

and the result is shown in Fig. 14b, for $\theta = 30°$. The projection of this rotated scatter plot on the x-axis is shown in Fig. 14c. This signal distribution is well described by a Gaussian function with a central value of 61.0 GeV and a relative width, σ/E, of 3.9%. This corresponds to $30\%/\sqrt{E}$. The narrowness of this distribution reflects the clustering of the data points around the axis of the locus in Fig. 14a.

We have applied exactly the same procedure for data taken at $+125$, $+80$, $+40$ and $+20$ GeV, and obtained similar results. In addition, the use of positive polarity beams allowed us to separate the data into proton and π^+ samples. Fig. 15 shows the Čerenkov *vs.* scintillation scatter plots for the 80 GeV π^+ (Fig. 15a) and proton (Fig. 15c) signals. These plots show a significant difference between the pion and proton signals. The average Čerenkov signal is about 10% larger for the pions than for the protons, a consequence of the absence of leading π^0s in the proton showers. However, using the intersection of the axis of the locus and the $C/S = 1$ point as the center of rotation, and the same rotation angle (30°) as for 60 GeV, the resulting signal distributions had about the same average value: 80.7 GeV for the pions (Fig. 15b) and 80.4 GeV for the protons (Fig. 15d). The widths of both distributions were also about the same: 2.60 for pions, 2.69 GeV for protons. Regardless of the differences between the production of π^0s (and thus of Čerenkov light) in these two types of showers, the signal distributions obtained after the dual-readout procedure applied here, were thus practically indistinguishable.

Also at the other mentioned energies, the average Čerenkov signals in the raw data were significantly smaller for protons than for pions, and these differences vanished after the described rotation procedure. The fact that the rotation angle used to achieve these results is independent of the particle type and the energy is consistent with Groom's observation that this angle only depends on the energy independent value of the χ parameter defined in Eq. (2) [14].

The results are summarized in Table 3, which lists for each type of particle the average value of the measured Čerenkov signals, the average signal after application of the dual-readout rotation method, the
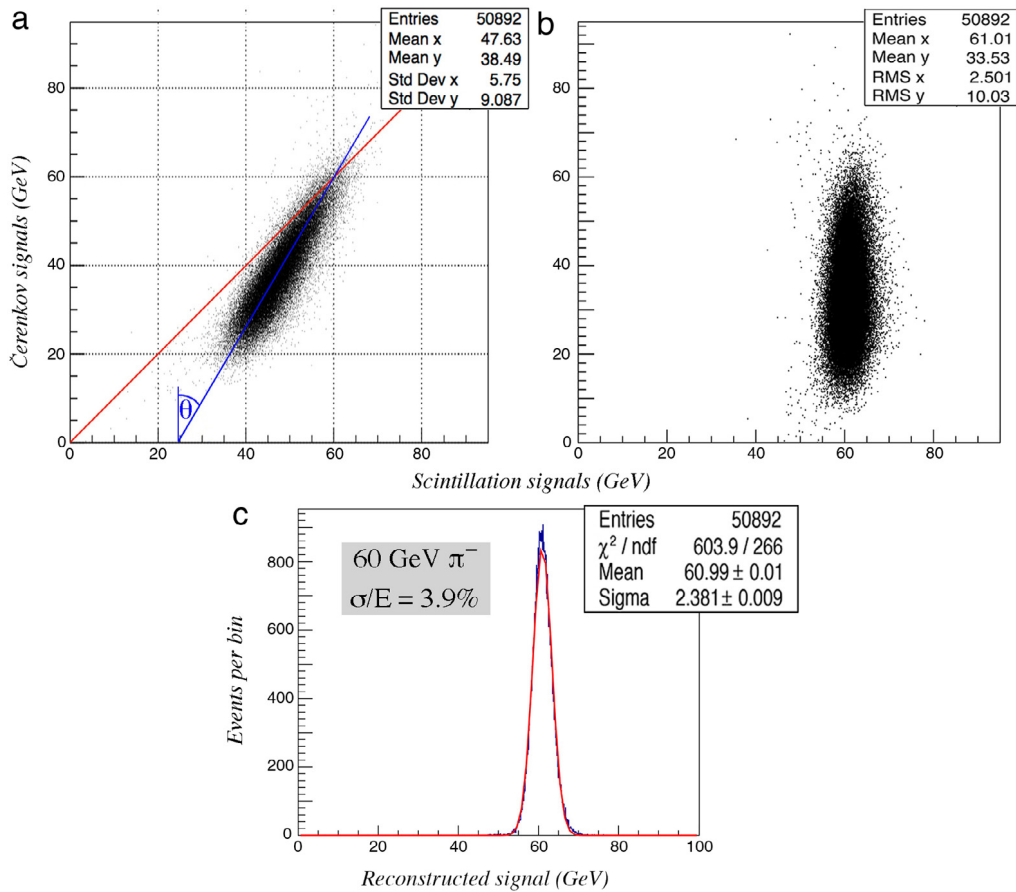
Fig. 14. Signal distributions of the RD52 Dual-Readout lead/fiber calorimeter for 60 GeV pions. Scatter plot of the two types of signals as recorded for these particles (a) and rotated over an angle $\theta = 30°$ around the point where the two lines from diagram a intersect (b). Projection of the latter scatter plot on the x-axis (c).

Table 3
The reconstructed energy and the energy resolution for proton and pion showers, measured with the rotation method. See text for details.

Particles	⟨Č signal⟩ (GeV)	⟨Reconstructed energy⟩ (GeV)	σ/E (%)	$\sigma/E \cdot \sqrt{E}$ (GeV) (%)
20 GeV π^+	8.00	20.5	6.61	29.5
20 GeV p	6.76	20.2	6.48	29.0
40 GeV π^+	21.7	41.3	4.49	28.4
40 GeV p	18.5	40.7	4.38	27.6
60 GeV π^-	38.5	61.0	3.90	30.2
80 GeV π^+	51.5	80.7	3.22	28.8
80 GeV p	47.1	80.4	3.34	29.9
125 GeV π^+	84.8	127	2.63	29.4
125 GeV p	77.8	126.5	2.85	31.9

fractional energy resolution (σ/E) and the fractional energy resolution multiplied with $\sqrt{E}$.

These results exhibit some very important features:

- The calorimeter is very linear, both for pion and for proton detection. The beam energy is correctly reconstructed at all energies within a few percent, using the energy scale for electrons, which were used to calibrate the signals. Fig. 16 shows the calorimeter response to protons and pions, *i.e.,* the average signal per unit deposited energy, as a function of energy. Variations of ±1% about the average value are indicated by the shaded band. The vertical scale is normalized to the electron response. The hadron signals are thus a few percent larger than those for em showers of the same energy.
- The reconstructed signal distributions are very narrow, narrower than those reported by any other detector we know of.

- The reconstructed signal distributions are very well described by Gaussian functions. This is illustrated in Fig. 17, which shows signal distributions for hadrons at the low and high end of the spectrum of particles studied here. The normalized χ^2 values varied between 1.02 and 2.27 for all particles listed in Table 3.
- The fractional width of the reconstructed signal distribution also scales very well as expected for an energy resolution dominated by Poissonian fluctuations. Over the full energy range of 20–125 GeV we find: $\sigma/E = (30\pm2\%)/\sqrt{E}$. This result is represented by the straight line in Fig. 18, which shows the experimental data points, separately for protons and pions, as a function of the beam energy.

4.3. The rotation method for multiparticle events

This method was used with the same rotation angle ($\theta = 30°$) for multiparticle events, samples of which were available for beam energies of +40, +60, +100 and +125 GeV. During these dedicated runs, the Interaction Target was installed in the beam line (see Fig. 3). Events were selected by requiring that the beam hadrons produced a signal compatible with a mip in the upstream PSD and a signal of at least 6 mip in the downstream scintillation counter. No distinction was made between protons and pions for this analysis. Otherwise, the conditions were identical to the ones used for the single-hadron analysis.

Fig. 19 shows an example of the signal distribution for 125 GeV multiparticle events obtained with the rotation method. This distribution shows similar features as those for single hadrons (Fig. 17): A rather narrow distribution, centered at approximately the correct (energy) value, well described by a Gaussian function. However, there are also some differences, which become more obvious when we look at the
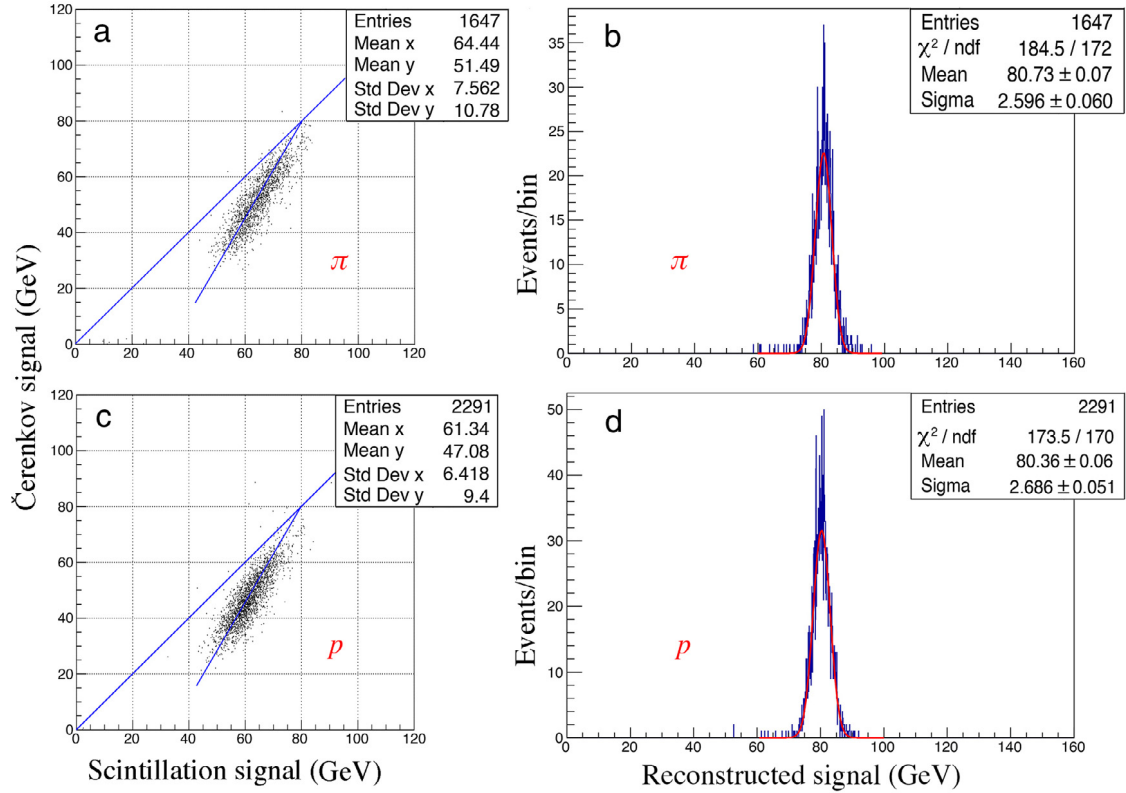
Fig. 15. Scatter plots of the Čerenkov *vs.* the scintillation signals from showers induced by 80 GeV π^+ (a) and 80 GeV protons (c). Projection of the rotated scatter plots on the x axis for the pions (b) and protons (d). The rotation procedure was identical to that used for 60 GeV π^- (Fig. 14).
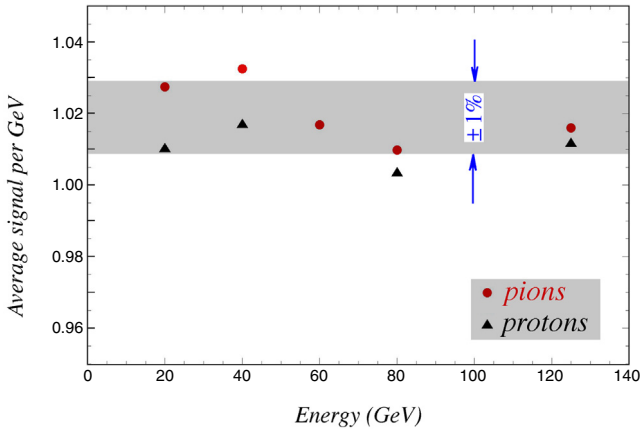

Fig. 16. The calorimeter response, *i.e.,* the average signal for protons and pions per GeV, as a function of energy. The vertical scale is normalized to the electron response.

results for all energies for which this analysis was carried out. These are listed in Table 4, and shown graphically in Fig. 20.

It turns out that the multiparticle signal distributions are clearly wider than those for single hadrons. However, in both cases, the fractional width scales with $E^{-1/2}$, without any significant deviations: 53%/$\sqrt{E}$ for "jets", *vs.* 30%/$\sqrt{E}$ (Fig. 20b). This indicates that only stochastic fluctuations contribute to this width. The reconstructed energies are also somewhat lower in the case of the multiparticle events, more so at low energy (Fig. 20a). Very substantial differences are observed in the size of the Čerenkov component, which is on average considerably smaller for the multiparticle events.

These features can be understood by realizing that the primary interaction of the beam particles took place at a distance of about 75 cm upstream of the calorimeter. Low-energy secondaries produced

in these interactions may have traveled at such large angles with the beam line that they physically missed the calorimeter, as well as the leakage counters surrounding the calorimeter. The effect of that is larger when the energy of the incoming beam particle is smaller. The increased side leakage is probably also the main factor responsible for the increased width of the signal distribution. The difference in the strength of the Čerenkov component most likely reflects the fact that the average energy fraction carried by the em component in hadronic showers increases with energy. Therefore, if the energy of the incoming beam particle is split between at least six secondaries (our trigger condition for multiparticle events), the total em energy fraction is likely to be smaller than when the beam particle enters the calorimeter and deposits its entire energy there in the form of a single hadronic shower.

4.4. Discussion

Notice that we have *not* used any knowledge about the energy of the beam particles in the rotation procedure described in the previous subsections. The coordinates of the rotation center were chosen on the basis of the *equality of the hadronic Čerenkov and scintillation signals*. This implies that the hadronic response at that point must be equal to that for electrons, which was used to set the energy scale for both types of calorimeter signals. The described method has thus allowed us to measure the energy of the beam particles with great precision. The average beam energy has been correctly reproduced within a few percent for all energies studied, the fractional width of the signal distribution scaled with $E^{-1/2}$ and, most interestingly, the dual-readout signal distributions were found to be essentially identical for protons and pions, despite the substantial differences between the signal distributions for these particles measured in the scintillation or Čerenkov channels. The latter aspect is a unique feature of dual-readout calorimetry. No other calorimeter we know of is capable of this. ATLAS has reported significant differences between the signal

Table 4

The reconstructed energy and the energy resolution for showers induced by pions and by multiparticle events ("jets"), measured with the rotation method. See text for details.

Particles	⟨Č signal⟩ (GeV)	⟨Reconstructed energy⟩ (GeV)	σ/E (%)	$\sigma/E \cdot \sqrt{E}$ (GeV) (%)
40 GeV π^+	21.7	41.3	4.49	28.4
40 GeV "jets"	14.7	37.9	8.32	52.6
60 GeV π^-	38.5	61.0	3.90	30.2
60 GeV "jets"	27.6	58.0	6.83	52.9
100 GeV "jets"	54.9	97.1	5.30	52.9
125 GeV π^+	84.8	127	2.63	29.4
125 GeV "jets"	69.0	122.6	4.79	53.6
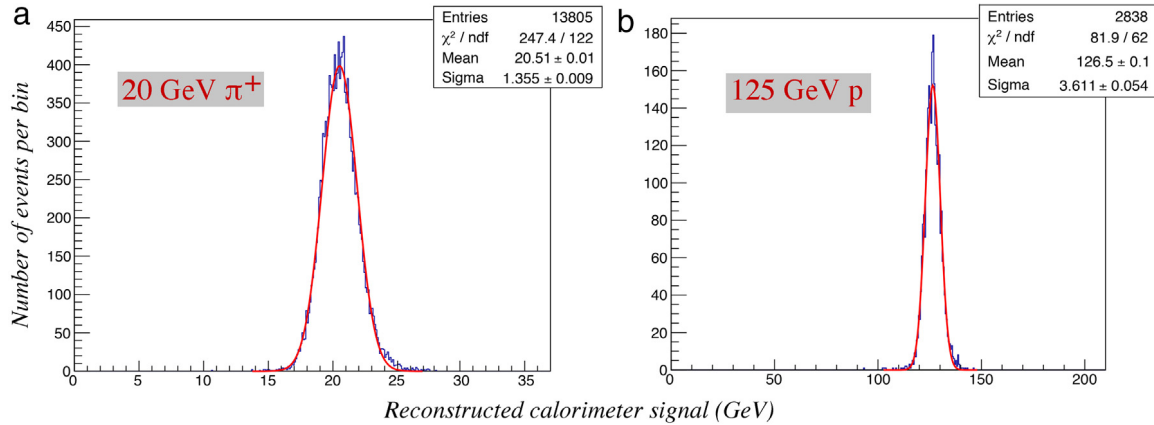
Fig. 17. Signal distributions for 20 GeV π^+ (a) and 125 GeV protons (b) obtained with the rotation method described in the text. The energy scale is set by electrons showering in this detector.
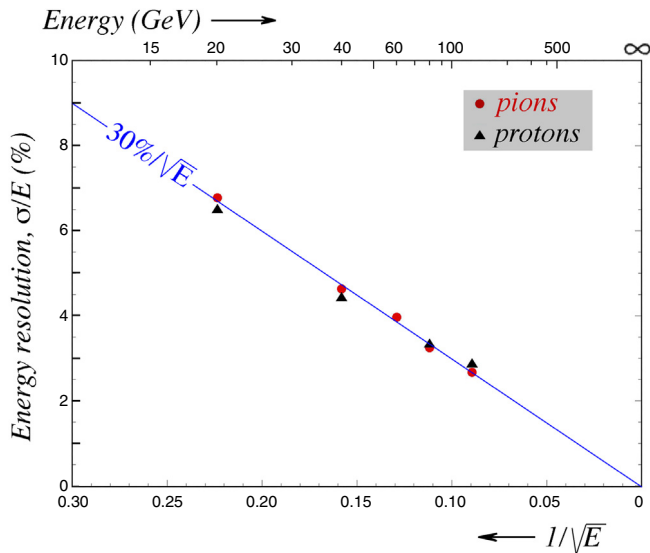

Fig. 18. The fractional width of the signal distribution, σ/E, as a function of energy, for pions and protons in the 20–125 GeV energy range. The line represents $\sigma/E = 30\%/\sqrt{E}$.

Fig. 19. Signal distribution for 125 GeV multiparticle events obtained with the rotation method described in the text. The energy scale is set by electrons showering in this detector.

distributions of protons and pions [15], but their "offline compensation" methods required prior knowledge of the particle type to eliminate these differences.

Yet, while we have managed to obtain very narrow signal distributions for the beam particles using only the calorimeter information, we do not think it is correct to interpret the relative width of these distributions as a measure for the precision with which the energy of an arbitrary particle absorbed in this calorimeter may be determined. The determination of the coordinates of the rotation point, and thus the energy scale of the signals, relied on the availability of an ensemble of events obtained for particles of the same energy. In practice, however,
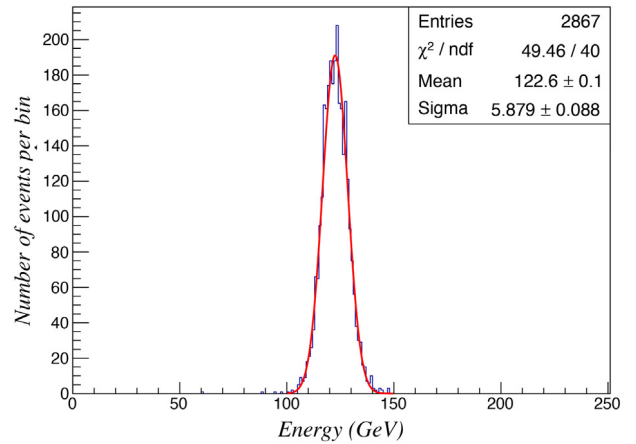
one is only dealing with one event, of unknown energy, and the described procedure can thus not be used in that case.

The DREAM Collaboration has developed a procedure to determine the energy of an unknown particle showering in the dual-readout calorimeter that is not affected by this problem. In this procedure, described in Section 3.1, the em shower fraction (f_{em}) of the hadronic shower is derived from the ratio of the Čerenkov and scintillation signals. Using the known e/h values of the two calorimeter structures, the measured signals can then be converted to the em energy scale ($f_{em} = 1$). The energy resolutions obtained with this method are worse than the ones given in this section, although it should be mentioned that they are dominated by incomplete shower containment and the associated leakage fluctuations, and are likely to improve considerably for detectors that are sufficiently large [10]. However, the same is
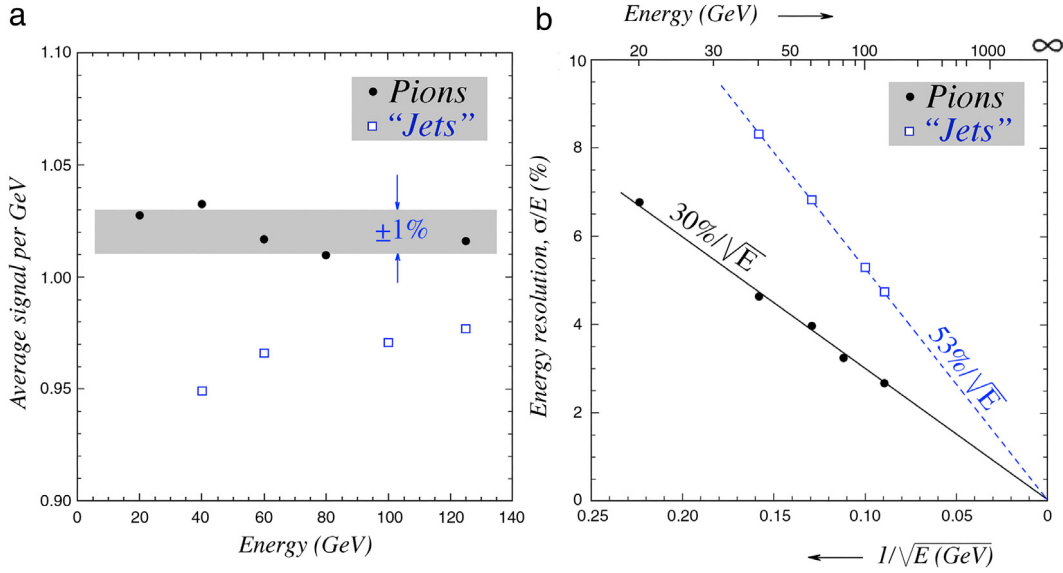
Fig. 20. The average calorimeter signal per GeV (a) and the fractional width of the signal distribution (b) as a function of energy, for single pions and multiparticle events ("jets"). Results are given for the dual-readout calorimeter signals, obtained with the rotation method.
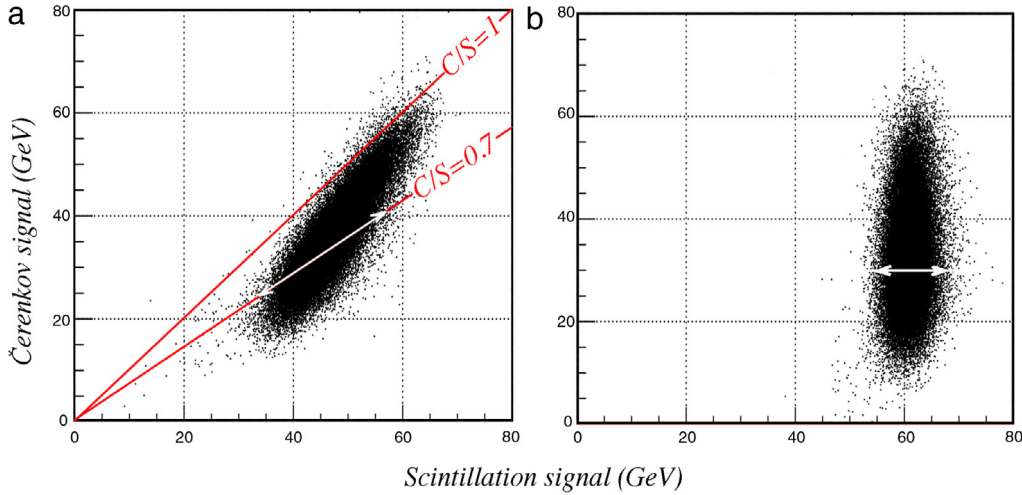

Fig. 21. Scatter plots of the Čerenkov *vs.* the scintillation signals from showers induced by mono-energetic hadrons (a). The arrow indicates the precision with which the em shower fraction, and thus the energy, of an individual particle can be determined on the basis of the measured ratio of the Čerenkov and scintillation signals, 0.7 in this example. The rotation procedure for an ensemble of mono-energetic pions leads to the scatter plot shown in diagram (b). The precision of the measurement of the width of that distribution is indicated by a white arrow as well.

probably true for the measurements of which the results are shown in Fig. 14. Fig. 21 graphically illustrates the difference between the values of the energy resolution obtained with the two methods discussed here. The precision of the energy measurement is represented by the arrows in the two diagrams.

The message we want to convey in this section is that one should not confuse the precision of the energy determination of a given event based on calorimeter signals alone with the width of a signal distribution obtained in a testbeam, since the latter is typically based on additional information that is not available in practice. In the example described above, this additional information derived from the fact that a large number of events generated by particles of the same energy were available. In other cases, additional information may be derived from knowledge of the particle energy.

5. Conclusions

We have studied the hadronic performance of a lead-based dual-readout fiber calorimeter with beams of pions and protons of different

energies, and with multiparticle events created by upstream interactions of these beam particles in a dedicated target. The assessment of the performance characteristics, and thus of the potential possibilities of this type of detector, was limited by the fact that the calorimeter was too small and used lead as absorber material. As has been pointed out elsewhere [16], a lower-Z absorber material such as copper would be much more suitable for this type of detector. However, we have not yet managed to identify a low-cost technique for mass production of the complicated absorber structure out of copper. On the other hand, lead could be extruded into the desired shape.

We have demonstrated that the hadronic energy resolution of the tested calorimeter was dominated by fluctuations in lateral shower leakage. We have tried to mitigate these effects with a crude and rather non-hermetic system of leakage counters surrounding the calorimeter. This certainly improved the energy resolution significantly, but not nearly enough to eliminate the leakage effects. The effects of leakage on the energy resolution became clear by selecting events in which no measurable leakage occurred. For these events, the measured resolution was comparable to that of the best compensating calorimeters ever built.

Similar performance was achieved with an analysis method in which we made use of the availability of an ensemble of events caused by particles of the same energy. The availability of two signals that provided complementary information about the showers made it possible to determine the energy of the particles, independent of any additional information. A simple rotation procedure then led to signal distributions with all the characteristics of an ideal calorimeter: Signal linearity, Gaussian response functions with a very narrow width that scaled with $E^{-1/2}$, and the same response for pions and protons, whose responses differed substantially when measured in the scintillation or Čerenkov channels.

With the exception of the energy resolution, similarly good performance was obtained with the standard dual-readout method, which can be applied for individual events. The width of the signal distribution which, as explained above, was dominated by lateral leakage fluctuations, was also in this case measured to be completely determined by stochastic fluctuations, as evidenced by the $E^{-1/2}$ scaling.

Acknowledgments

References

[1] N. Akchurin, et al., Nucl. Instrum. Methods Phys. Res. A A399 (1997) 202.
[2] All publications and other results obtained in the context of this project can be found at the RD52 website: http://www.phys.ttu.edu/~dream. http://dream.knu.ac.kr.
[3] N. Akchurin, et al., Nucl. Instrum. Methods Phys. Res. A A735 (2014) 130.
[4] A. Cardini, et al., Nucl. Instrum. Methods Phys. Res. A A808 (2016) 41.
[5] N. Akchurin, et al., Nucl. Instrum. Methods Phys. Res. A A735 (2014) 120.
[6] N. Akchurin, et al., Nucl. Instrum. Methods Phys. Res. A A537 (2005) 537.
[7] D.E. Groom, Nucl. Instrum Methods 572 (2007) 633.
[8] D. Acosta, et al., Nucl. Instrum. Methods Phys. Res. A A305 (1991) 55.
[9] F.G. Hartjes, R. Wigmans, Nucl. Instrum. Methods Phys. Res. A A277 (1989) 379.
[10] N. Akchurin, et al., Nucl. Instrum. Methods Phys. Res. A A762 (2014) 100.
[11] N. Akchurin, et al., Nucl. Instrum. Methods Phys. Res. A A408 (1998) 380.
[12] R. Wigmans, Calorimetry, Energy Measurement in Particle Physics, in: International Series of Monographs on Physics, vol. 107, Oxford University Press, 2000.
[13] G. Gaudio, R. Wigmans, Progress Report on the RD52 Project, CERN-SPSC-2013-012.
[14] C. Patrignani, et al. (Particle Data Group), Chin. Phys. C, C40 (2016) 100001. Section 34.9.2.
[15] P. Adragna, Nucl. Instrum. Methods Phys. Res. A A615 (2010) 158.
[16] R. Wigmans, Nucl. Instrum. Methods Phys. Res. A A718 (2013) 43.